Free-Standing and Single-Crystalline $Fe_{1-x}Mn_xSi$ Nanowires with Room-Temperature Ferromagnetism and Excellent Magnetic Response

Min-Hsiu Hung,[†] Chiu-Yen Wang,[†] Jianshi Tang,[‡] Ching-Chun Lin,[†] Te-Chien Hou,[†] Xiaowei Jiang,[‡] Kang L. Wang,[‡] and Lih-Juann Chen[†,*]

[†]Department of Materials Science and Engineering, National Tsing Hua University, Hsinchu, Taiwan, 30013, ROC and [‡]Device Research Laboratory, Department of Electrical Engineering, University of California, Los Angeles, California, 90095, United States

ABSTRACT

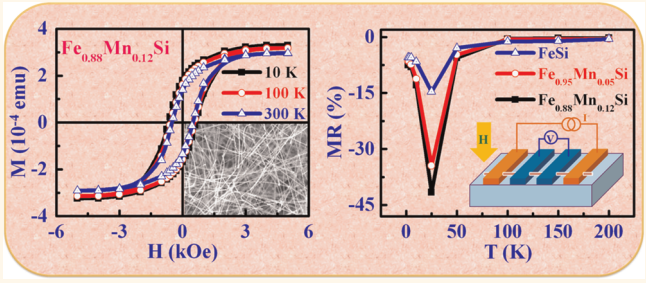

High-aspect-ratio $Fe_{1-x}Mn_xSi$ nanowires with room-temperature ferromagnetism were synthesized by a chemical vapor deposition (CVD) method in one step. This is the first report of ternary silicide nanowires using magnetic Mn ions to partially replace metal sites in the host matrix. Here we report the excellent magnetic characteristics of $Fe_{1-x}Mn_xSi$ nanowires, which exhibit strong ferromagnetism at room temperature and high magnetoresistance (MR) variation. As-synthesized $Fe_{1-x}Mn_xSi$ nanowires show a hyperbranched morphology and a spin-disorder behavior. The strong spin interaction in $Fe_{1-x}Mn_xSi$ nanowires, induced by the substitution of Fe sublattices for magnetic Mn ions, was revealed in the hysteresis loops. The magnetization versus magnetic field (M—H) curves of $Fe_{1-x}Mn_xSi$ nanowires are much less sensitive to the temperature variation from 10 to 300 K than those of FeSi nanowires. Remarkably, the excellent MR performance, —41.6% at 25 K with a magnetic field of 9 T, was demonstrated in an individual $Fe_{0.88}Mn_{0.12}Si$ nanowire.

KEYWORDS: silicide · nanowires · ferromagnetic · magnetic semiconductor · spin-disorder · magnetoresistance

In the recent decade, nanomaterials have attracted great attention due to their wide variety of morphologies, unique properties, and potential applications in electronic, optoelectronic, thermoelectric, and piezoelectronic devices.[1−6] Two approaches, top-down and bottom-up, have been extensively utilized to form structures in the nanoscale regime.[7,8] Among them, several high-aspect-ratio one-dimensional nanostructures (such as nanowires and nanobelts) possess outstanding physical properties with large surface-to-volume ratios compared with bulk materials.[9−12] Thermally stable and low-resistivity metal silicide nanowires have been widely used as interconnects for Si-based nanodevices owing to the maturity of complementary metal-oxide-semiconductor (CMOS) manufacturing techniques and the high compatibility with Si technology.[13,14] On the other hand, several binary and ternary silicide nanowires, like CoSi, FeSi, MnSi, and $Fe_{1-x}Co_xSi$, were suggested to have unusual magnetic behaviors with room-temperature (RT) ferromagnetism.[15−21] Therefore, ferromagnetic transition-metal silicide nanowires could be promising candidates in spintronic applications. However, the magnetic property of silicide nanowires is usually very sensitive to the measurement temperature. Appreciable RT ferromagnetism in silicide nanowires are difficult to achieve due to a significant decay in magnetization with increasing temperature.[16,21] Several semiconductors doped with 5% Mn were theoretically predicted to be ferromagnetic with a Curie temperatures (T_c) greater than 300 K.[22] In the previous work on dilute magnetic semiconductors (DMS), achieved by small quantity of magnetic atoms in substitution for the sublattice atoms of the nonmagnetic semiconductor matrix, the DMS could be a potential building block for spintronics.[23−29] However, the low solubility of magnetic dopants in the host structure increases the difficulty for practical applications. As a result, the development of an ideal material with considerable and stable ferromagnetism at RT is highly desirable.

* Address correspondence to ljchen@mx.nthu.edu.tw.

Received for review January 23, 2012 and accepted May 2, 2012.

Published online May 14, 2012
10.1021/nn300344k

In our search for a suitable magnetic semiconductor, Mn-doped FeSi nanostructures would be one of the promising candidates, although their magnetic performances have not been carefully studied yet. The narrow band gap semiconductor FeSi was found to exhibit metal−insulator transition behaviors.[30,31] On the other hand, some of the same B20-type silicide alloy compounds are of fundamental interest in magnetic behaviors that would make them suitable for spintronics. The unusual chiral magnet and Skyrmion lattice were reported for the $Fe_{1-x}Co_xSi$ and MnSi systems.[32−34] The large anomalous Hall-effect was also observed in bulk $Fe_{1-x}Co_xSi$.[28,29] Moreover, magnetic ordering was revealed in bulk $Mn_{1-x}Fe_xSi$ and $Mn_{1-x}Co_xSi$ alloys underlying a critical doping concentration.[35] These materials in the nanoscale-size regime have been further investigated in the transport properties or spintronic applications. For instance, spin polarization measurement of $Fe_{1-x}Co_xSi$ NWs was carried out by Andreev reflection spectroscopy, and the signatures of conical helimagnetic behavior were demonstrated with two-probe MnSi naonodevices.[15,16,36] The unique symbol of the temperature-dependent magnetic resistivity is that the maximum magnetoresistance (MR) does not occur at the lowest temperatiure.[15,16,37] For bulk single-crystalline FeSi and MnSi nanowires, the maximum MR were observed at 0.7 and 35 K, respectively.[15,16,37] In crystallography, a continuous solid solution of $Fe_{1-x}Mn_xSi$ could be formed by isostructural FeSi and MnSi in the overall regime. Therefore, $Fe_{1-x}Mn_xSi$ would be a ferromagnetic semiconductor with a high Curie temperature, and such nanoscale material is believed to be a promising building block for Si-based spintronic devices with fascinating magnetic properties.

RESULTS AND DISCUSSION

To control the composition of $Fe_{1-x}Mn_xSi$ nanowires, various ratios of the mixed source with $MnCl_2$ and $FeCl_2$ powders were used similar to the synthesis of $Fe_{1-x}Co_xSi$ nanowires.[18,21] The morphology, phase identification, structural analysis, and chemical composition of the reaction product were characterized with SEM, grazing incident X-ray diffraction (GIXRD), and transmission electron microscope (TEM).

Figure 1a shows the typical top view SEM image of $Fe_{0.88}Mn_{0.12}Si$ nanowires with 40−80 nm in diameter and tens of micrometer in length. The GIXRD spectra (2θ = 1°) of as-prepared $Fe_{1-x}Mn_xSi$ and pure FeSi nanowires are shown in Figure 1b. All peaks can be ascribed to the FeSi phase (JCPDF file 38-1397). The $\Delta(2\theta)$ of 0.1° was obtained, indicating about 10% Mn concentration in $Fe_{1-x}Mn_xSi$ nanowires in the further investigation of diffraction peaks at the higher angle in (311) plane. Figure 2a is the low-magnification TEM image of an individual nanowire with a diameter of 50 nm. The surface oxide of silicide nanowires was removed by dipping the nanowires into diluted hydrofluoric (HF) solution. For $Fe_{1-x}Mn_xSi$ alloys, FeSi and MnSi belong to the same structural type (space group $P2_13$) with a lattice constant of 0.4487 nm (JCPDF file 38-1397) for FeSi and 0.4558 nm (JCPDF file 65-5272) for MnSi. The magnetic Mn ion in substitution for the Fe sublattice in $Fe_{1-x}Mn_xSi$ (traditional metal site, hole-doped) not only provides a localized spin but also acts as an acceptor at the same time.[38] The selected area electron diffraction (SAED) pattern with the $[1\bar{1}1]$ zone axis is shown in Figure 2b and can be ascribed to the cubic B20 type $Fe_{1-x}Mn_xSi$ phase. In addition, it demonstrates that the preferential growth of the nanowire is along the [011] direction. As shown in the high-resolution TEM (HRTEM) image in Figure 2c, the host structure for the $Fe_{1-x}Mn_xSi$ nanowire is single-crystalline without any linear or planar defects. If the $Fe_{1-x}Mn_xSi$ nanowire is considered as a perfect alloy formed by FeSi and MnSi, the expected interspacing for $Fe_{1-x}Mn_xSi$ (101) planes would fall between 0.317 and 0.322 nm. The corresponding *d*-spacing of 0.318 nm obtained from the HRTEM image for a typical nanowire agrees well with the predicted values.

To further investigate the chemical composition in the $Fe_{1-x}Mn_xSi$ nanowires, the energy dispersive spectrometer (EDS) measurement was performed on several individual nanowires in TEM. The EDS spectrum shown in Figure 2d indicates the presence of only three elements, that is, Fe, Mn, and Si, in the nanowire and the C and Cu signals are from the copper holder and the copper grid with carbon film windows. The atomic ratio of ([Fe]+[Mn])/[Si] is close to 1, which is consistent with the host structure of FeSi. The *x* value, the Mn content in $Fe_{1-x}Mn_xSi$ nanowires, is defined by the formula [Mn]/([Mn]+[Fe]). The obtained average *x* value of 13 nanowires using the EDS spectrum is 0.12 ± 0.02. The TEM−EDS mapping is shown in Figure 3, and the result suggests that the elements of Fe, Mn. and Si are also distributed homogeneously within the nanowire. FeSi and $Fe_{0.95}Mn_{0.05}Si$ nanowires were acquired using different mixing weight percentages of $FeCl_2$ and $MnCl_2$ powders. The corresponding data (shown in Supporting Information, Figures S1 and S2) about the structure analysis and atomic ratios of nanowires were also obtained by SEM and TEM. The SEM image in Figure S1 exhibits the hyperbranched growth of $Fe_{1-x}Mn_xSi$ nanowires, and the growth morphology was also observed for the FeSi nanowires of the B20 type structure.[39] The absence of metal catalysts at the tips of nanowires suggested that a vapor−solid (VS) mechanism was operating the self-assembled growth of $Fe_{1-x}Mn_xSi$ nanowires. Recently, various metal halide or organometallic powders have been used to synthesize a number of metal silicide nanostructures *via* a CVD method.[12−21,40] At the setup temperature in the downstream region, reactions of

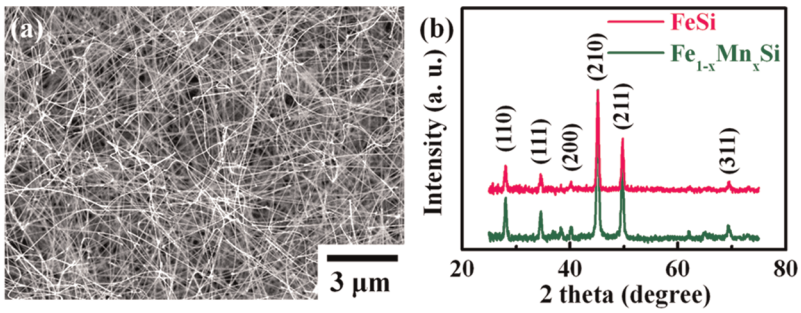

Figure 1. Morphology and structural analysis of as-grown $Fe_{0.88}Mn_{0.12}Si$ nanowires. (a) Top view SEM image of free-standing nanowires that are 40−80 nm in diameter and tens of micrometers in length. (b) The GIXRD spectra ($2\theta = 1°$) of as-prepared $Fe_{1-x}Mn_xSi$ and pure FeSi nanowires. All peaks can be ascribed to the FeSi phase. The $\Delta(2\theta)$ of 0.1° in the (311) plane was obtained to indicate a concentration of about 10% Mn in $Fe_{1-x}Mn_xSi$ nanowires.

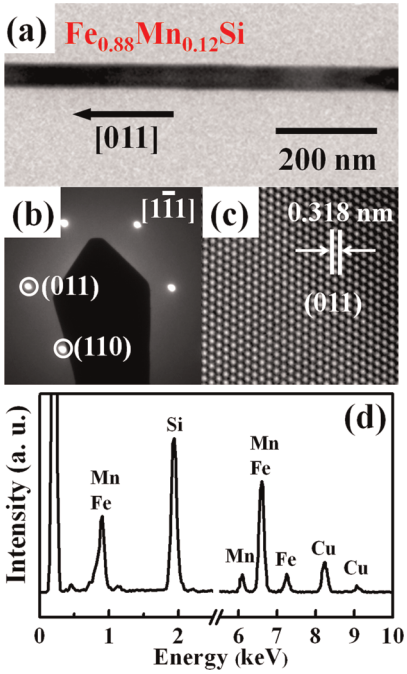

Figure 2. (a) Low-magnification TEM image of a $Fe_{0.88}Mn_{0.12}Si$ nanowire. (b) SAED pattern with the [1$\bar{1}$1] zone axis is indexed for a single crystalline $Fe_{1-x}Mn_xSi$ with cubic B20 structure. (d) HRTEM image shows a *d*-spacing of 0.318 nm in agreement with the interplanar (011) spacing. (e) TEM-EDS spectrum confirms the chemical composition of a representative $Fe_{0.88}Mn_{0.12}Si$ nanowire.

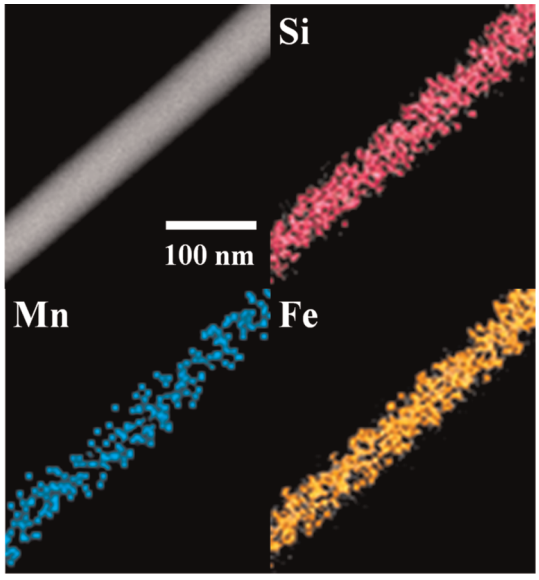

Figure 3. TEM−EDS mapping for each element in a single $Fe_{0.88}Mn_{0.12}Si$ nanowire. The result suggests that the elements of Fe, Mn, and Si are distributed homogeneously within the nanowire.

vapors of both metal halides and silicon substrates may follow two possible pathways:

$$2(Mn, Fe)Cl_{2(g)} + 3Si_{(s)} \rightarrow 2Fe_{1-x}Mn_xSi_{(s)} + SiCl_{4(g)}$$

$$SiCl_{4(g)} + (Mn, Fe)Cl_{2(g)} \rightarrow Fe_{1-x}Mn_xSi + 3Cl_{2(g)}$$

The optimized temperature ranges for growing iron monosilicide and manganese monosilicide nanowires were reported to be 850−1100 °C and 875−950 °C, respectively.[16,20] Taking the experimental setup of our CVD equipment into consideration, 850 °C was found to be the optimal reaction temperature to grow high-aspect-ratio and dense nanowires. The highest Mn concentration for $Fe_{1-x}Mn_xSi$ nanowires was 12% in our work, even if a mixed powder of $MnCl_2$:$FeCl_2$ = 9 in weight ratio was used. In addition, a very low density of MnSi nanowires could be synthesized if only $MnCl_2$ powders were used as the precursor under the same growth condition, as examined with SEM. In *et al.* also reported the similar result in growing ternary $Fe_{1-x}Co_xSi$ nanowires.[21] Comparing to the quantity of FeSi nanowires and MnSi nanowires in a unit area from previous works, the FeSi nanowire density was much higher than the latter. Therefore, the reason for low Mn contents in our $Fe_{1-x}Mn_xSi$ nanowires could be because it is more difficult for the nucleation of MnSi nanowires than that of FeSi nanowires. On the other hand, the reaction temperature, which is a little lower than before, may be a further reason for not readily overcoming the growth barrier.[16]

Although several studies of binary silicides have been reported, especially in FeSi and MnSi, this is the

first investigation on ternary metal silicide nanowires as ferromagnetic semiconductor that was caused by doping the magnetic Mn ion into metal silicide nanowires. MnSi nanowires were reported to show helimagnetic behaviors with a T_C of about 30 K.[15,16] FeSi nanowires were demonstrated to display extraordinary RT magnetic properties due to the spin interaction of surface-induced dangling bonds.[19,20] The $Fe_{1-x}Mn_xSi$ nanowires are of interest in studying the correlation of the temperature-dependent magnetization with the varied Mn contents. In addition, lightly Co-doped FeSi and MnSi nanowires were reported to display unusual helimagnetic behavior.[15,38] Figure 4 shows the schematic plots of field-cooled (FC) and zero-field-cooled (ZFC) magnetization for $Fe_{1-x}Mn_xSi$ nanowires as a function of temperature, *M*(T), characterized by superconducting quantum interference device magnetometer (SQUID). The detailed magnetic characteristics of FeSi NWs are summarized as follows: first, the peaks were obviously found in both ZFC curves under an applied field of 100 and 1000 Oe, respectively. Second, the apparent shift between the two peaks of ZFC curves was also displayed under different applied fields. Third, FC and ZFC curves completely converged above the freezing temperature (T_F, as marked in Figure 4a) up to RT. Figure 4b shows several **M**−**H** curves of the FeSi nanowires at 10, 100, and 300 K. Furthermore, the magnetization (**M**) *versus* measurement temperature (**M**−*T*) curves and **M**−**H** hysteresis loops for $Fe_{0.95}Mn_{0.05}Si$ and $Fe_{0.88}Mn_{0.12}Si$ nanowire ensembles are shown in Supporting Information Figure S3 and Figure 3c,d, respectively. Fourth, comparing the ZFC curves for different Mn contents (0%, 5%, and 12%) using the same measurement parameter, the broadened peak with a higher Mn concentration indicates the existence of strong interactions in the whole matrix. The freezing temperature of the FC curve for $Fe_{1-x}Mn_xSi$ NWs cannot be clearly distinguished. As a result, the magnetization gradient in ZFC curves was slight in the temperature range of 10−300 K. Such material, possessing the several features as remarked above, would be conceivably associated with spin disorder in a nanowire system. On the other hand, magnetic hysteresis loops of the as-synthesized $Fe_{1-x}Mn_xSi$ nanowires were observed explicitly. Assembled FeSi, $Fe_{0.95}Mn_{0.05}Si$, and $Fe_{0.88}Mn_{0.12}Si$ nanowires all demonstrate ferromagnetic characteristics above RT. Typically, the magnetization of many ferromagnetic nanowire systems, such as FeSi nanowires, was found to be extremely sensitive to the change in entropy with temperature.[19,20] However, the **M**−**H** loops in Supporting Information Figure S3 and Figure 4d illustrate the presence of strong spin interaction in the $Fe_{1-x}Mn_xSi$ nanowires ($x \neq 0$) because the **M**−**H** curves are almost identical at different temperatures.

It is necessary to carry out further quantitative analysis to better reveal magnetic behaviors. The coercive field (H_C) and residual magnetization (M_R) were extracted from the **M**−**H** hysteresis loops on an enlarged scale near the zero magnetic field. In Figure 5a, H_C was observed to increase with Mn concentrations. The intrinsic value of H_C/H_{C_0} (H_{C_0} denotes the maximum H_C at 10 K.) was introduced to eliminate the effect of diameter, length, and density of $Fe_{1-x}Mn_xSi$ nanowires with various Mn-content. Figure 5b reveals the temperature-dependent H_C/H_{C_0} of FeSi, $Fe_{0.95}Mn_{0.05}Si$, and $Fe_{0.88}Mn_{0.12}Si$ nanowires, respectively. The higher the Mn-contents of $Fe_{1-x}Mn_xSi$ nanowires, the more slowly the relative value of H_C/H_{C_0} decreases with increasing temperature. Teran *et al.* has reported similar results in the ferromagnetic semiconductor system with a magnetic-field-induced ferromagnetic order.[27] In addition, the RKKY interaction could be the dominant spin interaction in DMS.[22,28] Even though the influence of carrier−carrier interaction is expected to decrease by static disorders in thermodynamics, $Fe_{1-x}Mn_xSi$ nanowires with higher acceptor concentrations show a stronger exchange coupling effect. These inferences were in agreement with our results, indicating that $Fe_{0.88}Mn_{0.12}Si$ nanowires with the strongest spin interaction have the highest thermal stability.

The electrical transport properties and MR behaviors of an individual $Fe_{0.88}Mn_{0.12}Si$ nanowire are shown in Figure 6 panels a and 6b, respectively. The electrical response of an individual nanowire was acquired with a four-terminal device. The devices for transport measurements were fabricated by defining multiple metal contacts of 30 nm Cr and 120 nm Au with e-beam lithography (EBL). The inset in Figure 6a shows the SEM image of a typical nanowire device. The contact resistance could be excluded using four-probe *I*−*V* measurements. The electrical resistance was extracted from the slope of the *I*−*V* curve to estimate the resistivity. The calculated resistivity of $Fe_{0.88}Mn_{0.12}Si$ nanowire is 0.41 ± 0.08 mΩ-cm in average for 12 nanowire devices. The value is close to the data reported in previous studies for FeSi and MnSi nanowires.[15,20,41] The MR measurements ranged between 2 and 200 K for a single $Fe_{1-x}Mn_xSi$ nanowire and were carried out at various magnetic fields up to 9 T. The MR ratio is denoted as $MR = [R_{(H)} - R_{(0)}]/R_{(0)}$, where $R_{(H)}$ and $R_{(0)}$ are the resistance at an applied field and zero field, respectively. Recently, the MR features of transition-metal silicide nanowires were discussed extensively. Owing to the surface spin with the reduced coordination, the CoSi nanowire with a high surface-to-volume ratio was found to exhibit ferromagnetic property at RT. The negative MR effect (about −4% at 2 K with an applied field of 9 T) was obtained in a single CoSi nanowire device.[22] The maximum MR performance is usually achieved at the lowest temperature. However,

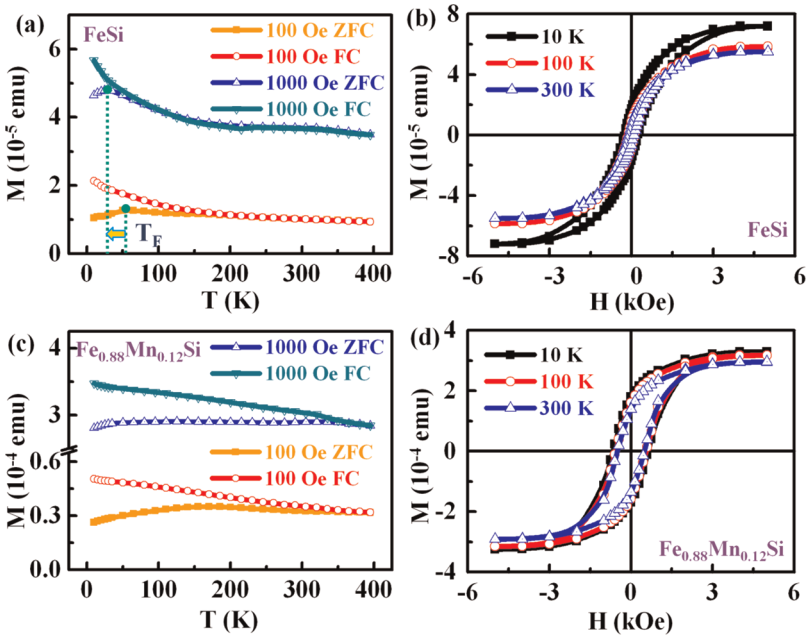

Figure 4. Magnetic properties of the as-grown $Fe_{1-x}Mn_xSi$ nanowires measured by SQUID. (a) The freezing temperature T_F denotes the corresponding temperature of the peak in the ZFC curve. The apparent peak shift between two ZFC curves was also displayed under different applied fields. (b) The M−H curves of FeSi nanowires at 10, 100, and 300 K. (c) The temperature-dependent magnetization of the $Fe_{0.88}Mn_{0.12}Si$ nanowires in FC and ZFC conditions under applied fields of 100 and 1000 Oe, respectively. (d) The M−H curves of $Fe_{0.88}Mn_{0.12}Si$ nanowires at 10 K, 100 K, and 300 K. The results also show that the M−H curves are almost overlapping at different temperatures.

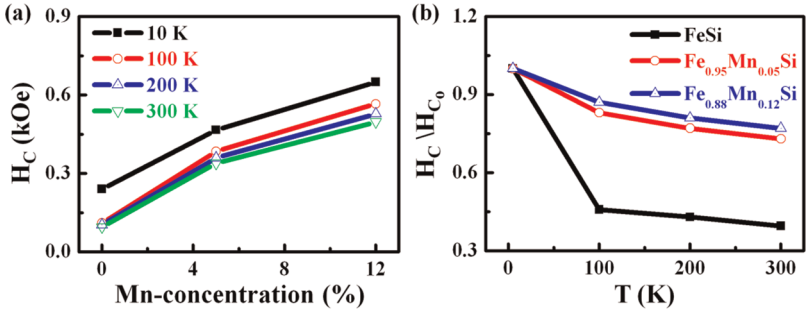

Figure 5. (a) The schematic plots of H_C as a function of Mn-concentration of $Fe_{1-x}Mn_xSi$ nanowires at different temperatures. (b) H_C/H_{C0} *vs* T curves of FeSi, $Fe_{0.95}Mn_{0.05}Si$ and $Fe_{0.88}Mn_{0.12}Si$ nanowire ensembles. The coercive field (H_C) was obtained from the partially enlarged M−H hysteresis loops near zero magnetic field.

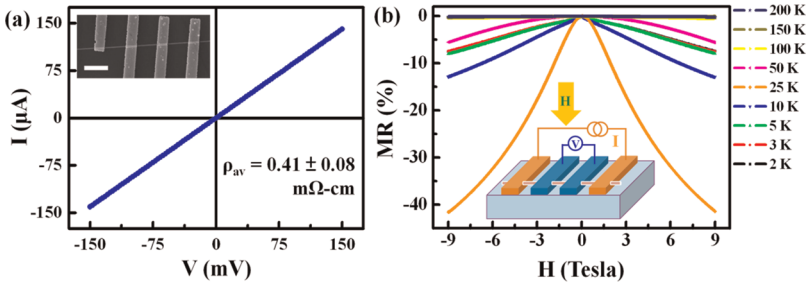

Figure 6. (a) The four-terminal measurement of an individual $Fe_{0.88}Mn_{0.12}Si$ nanowire device at RT. The inset is the SEM image of a $Fe_{0.88}Mn_{0.12}Si$ nanowire device fabricated with a standard EBL process. The scale bar equals 2 μm. The estimated resistivity is 0.41 $\pm$ 0.08 mΩ-cm from 12 nanowire devices. (b) MR *vs* H curves of a single $Fe_{0.88}Mn_{0.12}Si$ nanowire operating at various temperatures. The maximum MR value was obtained at 25 K and 9 T.

MnSi and $Co_2Si_{0.5}Ge_{0.5}$ nanowires were suggested to have helimagnetic order and spin-glass like behavior, respectively.[15,42] The maximum MR value (approximately −5% at 35 K and 1.5 T for MnSi and −11.7%

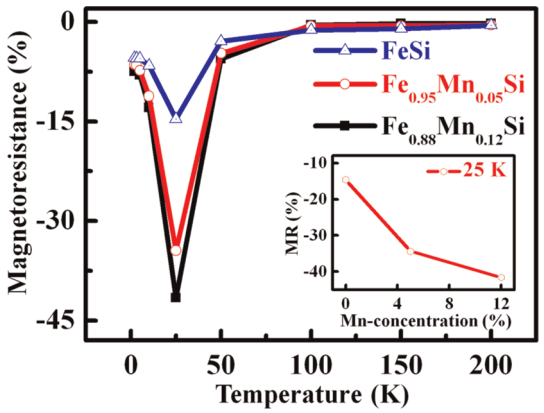

Figure 7. The temperature-dependent MR ratios for FeSi, $Fe_{0.95}Mn_{0.05}Si$ and $Fe_{0.88}Mn_{0.12}Si$ nanowire. The MR *vs* Mn content within $Fe_{1-x}Mn_xSi$ nanowires plot is shown in the inset. The maximum magneto-transport properties of single FeSi, $Fe_{0.95}Mn_{0.05}Si$ and $Fe_{0.88}Mn_{0.12}Si$ nanowire devices are −14.6%, −34.4%, and −41.6%, respectively. Moreover, the MR ratios were found to increase with Mn concentrations.

at 10−25 K and 8 T for $Co_2Si_{0.5}Ge_{0.5}$) was not observed at the lowest measured temperature.[15,42] In addition, the β-$FeSi_2$ nanowires were first reported to possess a maximum MR value (6% at 200 K and 9 T) above 77 K.[43] In our case as shown in Figure 6b, it is significant to find the unsaturated MR ratio of −41.6% at the field of 9 T at 25 K.

Figure 7 shows the temperature-dependent MR of an individual $Fe_{1-x}Mn_xSi$ nanowire device with different Mn contents measured in a quantum design physical property measurement system (PPMS). The MR reaches the maximum variation value at around 25 K with an applied field of 9 T. The inset in Figure 7 shows the plot of the MR *versus* Mn concentrations in $Fe_{1-x}Mn_xSi$ nanowires at 25 K. The maximum MRs of the individual FeSi, $Fe_{0.95}Mn_{0.05}Si$ and $Fe_{0.88}Mn_{0.12}Si$ nanowire devices are −14.6%, −34.4%, and −41.6%, respectively. The MR value of −41.6% is a new record among silicide nanowires up to the present time. (Detailed comparisons of MR behaviors are listed in Table 1.) Furthermore, the MR signature of $Fe_{1-x}Mn_xSi$ nanowires shows a similar tendency with bulk single-crystalline FeSi as with MnSi nanowires.[15,16,37] The MR ratios were found to increase with Mn-concentrations due to the enhancement of the p−d interaction.[27] The MR result is consistent in the SQUID data as mentioned above and in several previous reports.[37,44] On the basis of the temperature-insensitive **M**−**H** curves below 300 K and the excellent MR behavior, $Fe_{1-x}Mn_xSi$ nanowires with strong ferromagnetism are promising to be applicable in Si-based magnetic nanodevices.

TABLE 1. The Ferromagnetic Silicide Nanowires (Phase, MR Ratio, Applied Field, Temperature) Are Compared with the Present Work

phase	MR ratio (%)	applied field (T)	temperature (K)
β-$FeSi_2$[42]	6	9	200
$Fe_{0.56}Co_{0.44}Si$[23]	8.7	9	2
MnSi[20]	−5.3	1.5	35
MnSi[21]	−20	9	30
CoSi[22]	−4	9	2
$Co_2Si_{0.5}Ge_{0.5}$[41]	11.7	8	10−25
Co_2Si[44]	−0.09	9	10
FeSi[a]	−14.6	9	25
$Fe_{0.88}Mn_{0.12}Si$[a]	−41.6	9	25

[a] Values from the present work.

SUMMARY AND CONCLUSIONS

Free-standing and single-crystalline $Fe_{1-x}Mn_xSi$ nanowires were synthesized in one step by using a two hot-zone furnace through a spontaneous thermal CVD method. The cubic B20 type $Fe_{1-x}Mn_xSi$ phase was verified by the HRTEM analysis and SAED pattern. The Mn contents x in $Fe_{1-x}Mn_xSi$ nanowires were determined to be 0, 0.05, and 0.12 for three different ratios of mixed precursors *via* the TEM-EDS analysis. For the first time, we show ferromagnetic ternary silicide nanowires with the substitution of Fe with magnetic Mn, and the magnetic behavior was systematically discussed. Room-temperature ferromagnetic property and unique spin-disorder behavior of $Fe_{1-x}Mn_xSi$ nanowires were found with SQUID. The significant influence of strong carrier−carrier interaction was introduced to reduce the temperature sensitivity of the magnetization. As a result, the field-dependent magnetization shows similar ferromagnetic behaviors within the whole temperature range between 10 and 300 K. The electrical transport and MR measurements were carried out *via* the use of four-terminal devices. The $Fe_{0.88}Mn_{0.12}Si$ nanowire with a record high MR value of −41.6% at 25 K and 9 T would be a promising candidate for application in Si-based magnetic nanodevices.

EXPERIMENTAL SECTION

Free-standing and single-crystalline $Fe_{1-x}Mn_xSi$ nanowires were synthesized in a two-zone furnace through a CVD method. To obtain different Mn/Fe atomic ratio for $Fe_{1-x}Mn_xSi$ nanowires, we used a different mixed ratio of $MnCl_2/FeCl_2$ (0, 5, and 9 in weight). The (001) silicon substrate was cleaned with 1% buffered HF prior to loading into the downstream region of the furnace. The front and back heating centers which were 20 cm apart were heated from RT to 725 and 850 °C, respectively. The reaction at atmospheric pressure was kept for 2 h with a constant Ar flow of 150 SCCM (SCCM denotes cubic centimeter per minute at STP), and then the furnace was cooled down to RT slowly. The morphology and structural analysis of the reaction product was carried out with a field-emission SEM (JEOL JSM-6500F) and a GIXRD, respectively. The phase, chemical composition, and high resolution image of nanostructures were obtained by using a 200 kV TEM (JEOL JSM-2010) equipped with an EDS. The elemental mapping for a single nanowire was

collected by TEM-EDS (JEOL JEM-3000F) with an accelerating voltage of 300 kV. As-synthesized nanowires were dispersed on a Si substrate with 100 nm Si_3N_4 and patterned by standard EBL process to fabricate four-terminal devices. Before the deposition of 30 nm/120 nm of Cr/Au electrodes, the sample was dipped into a diluted HF solution for 5 s and cleaned with D.I. water for several times to remove the native oxide in the contact region. Electrical transport properties at room temperature and atmospheric pressure were measured by using Agilent B1500A semiconductor device analyzer (SDA) with four-probe station. The magnetic properties were characterized with a SQUID magnetometer. The magneto-transport properties of $Fe_{1-x}Mn_xSi$ nanowires were collected with PPMS at various temperatures and magnetic fields.

Conflict of Interest: The authors declare no competing financial interest.

Acknowledgment. The work was supported by the National Science Council through Grant No. NSC 98-2221-E-007-104-MY3. This study was in part supported by Western Institution of Nanoelectronics (WIN) and Focus Center on Functional Engineered Nano Architectonics (FENA).

Supporting Information Available: Additional figures as described in the text. This material is available free of charge *via* the Internet at http://pubs.acs.org.

REFERENCES AND NOTES

1. Chen, K. C.; Wu, W. W.; Liao, C. N.; Chen, L. J.; Tu, K. N. Observation of Atomic Diffusion at Twin-Modified Grain Boundaries in Copper. *Science* **2008**, *321*, 1066–1069.
2. Zhong, Z.; Wang, D.; Cui, Y.; Bockrath, M. W.; Leiber, C. M. Nanowire Crossbar Arrays as Address Decoders for Integrated Nanosystems. *Science* **2003**, *302*, 1377–1379.
3. Chen, L. J. Metal Silicides: An Integral Part of Microelectronics. *J. Miner., Met., Mater. Soc.* **2005**, *57*, 24–30.
4. Ko, H.; Takei, K; Kapadia, R.; Chuang, S.; Fang, H.; Leu, P. W.; Ganapathi, K.; Plis, E.; Kim, H. S.; Chen, S. Y.; *et al.* Ultrathin Compound Semiconductor on Insulator Layers for High-Performance Nanoscale Transistors. *Nature* **2010**, *468*, 286–289.
5. Hahn, C.; Zhang, Z.; Fu, A.; Wu, C. H.; Hwang, Y. J.; Gargas, D. J.; Yang, P. Epitaxial Growth of InGaN Nanowire Arrays for Light Emitting Diodes. *ACS Nano* **2011**, *5*, 3970–3976.
6. Hochbaum, A. I.; Chen, R.; Delgado, R. D.; Liang, W.; Garnett, E. C.; Najarian, M.; Majumdar, A.; Yang, P. Enhanced Thermoelectric Performance of Rough Silicon Nanowires. *Nature* **2008**, *451*, 163–167.
7. Pan, Z. W.; Dai, Z. R.; Wang, Z. L. Nanobelts of Semiconducting Oxides. *Science* **2001**, *291*, 1947–1949.
8. Morales, A. M.; Lieber, C. M. A Laser Ablation Method for the Synthesis of Crystalline Semiconductor Nanowires. *Science* **1998**, *279*, 208–211.
9. Huang, C. T.; Song, J.; Lee, W. F.; Ding, Y.; Gao, Y.; Hao, Y.; Chen, L. J.; Wang, Z. L. GaN Nanowire Arrays for High-Output Nanogenerators. *J. Am. Chem. Soc.* **2010**, *132*, 4766–4771.
10. Chen, M. T.; Lu, M. P.; Wu, Y. J.; Song, J.; Lee, C. Y.; Lu, M. Y.; Chang, Y. C.; Chou, L. J.; Wang, Z. L.; Chen, L. J. Near UV LEDs Made with *in Situ* Doped p−n Homojunction ZnO Nanowire Arrays. *Nano Lett.* **2010**, *10*, 4387–4393.
11. Jung, Y.; Lee, S. H.; Ko, D. K.; Agarwal, R. Synthesis and Characterization of $Ge_2Sb_2Te_5$ Nanowires with Memory Switching Effect. *J. Am. Chem. Soc.* **2006**, *128*, 14025–14027.
12. Hou, T. C.; Han, Y. H.; Lo, S. C.; Lee, C. T.; Ouyang, H.; Chen, L. J. Room-Temperature Ferromagnetism in $CrSi_2$(core)/SiO_2(shell) Semiconducting Nanocables. *Appl. Phys. Lett.* **2011**, *98*, 193104.
13. Lee, C. Y.; Lu, M. P.; Liao, K. F.; Lee, W. F.; Huang, C. T.; Chen, S. Y.; Chen., L. J. Free-Standing Single-Crystal $NiSi_2$ Nanowires with Excellent Electrical Transport and Field Emission Properties. *J. Phys. Chem. C* **2009**, *113*, 2286–2289.
14. Tsai, C. I.; Yeh, P. H.; Wang, C. Y.; Wu, H. W.; Chen, U. S.; Lu, M. Y.; Wu, W. W.; Chen, L. J.; Wang, Z. L. Cobalt Silicide Nanostructures: Synthesis, Electron Transport, and Field Emission Properties. *Cryst. Growth Des.* **2009**, *9*, 4514–4518.
15. Higgins, J. M.; Ding, R.; DeGrave, J. P.; Jin, S. Signature of Helimagnetic Ordering in Single-Crystal MnSi Nanowires. *Nano Lett.* **2010**, *10*, 1605–1610.
16. Seo, K.; Yoon, H.; Ryu, S. W.; Lee, S.; Jo, Y.; Jung, M. H.; Kim, J.; Choi, Y. K.; Kim, B. Itinerant Helimagnetic Single-Crystalline MnSi Nanowires. *ACS Nano* **2010**, *4*, 2569–2576.
17. Seo, K.; Varadwaj, K. S. K.; Mohanty, P.; Lee, S.; Jo, Y.; Jung, M. H.; Kim, J.; Kim, B. Magnetic Properties of Single-Crystalline CoSi Nanowires. *Nano Lett.* **2007**, *7*, 1240–1245.
18. Schmitt, A. L.; Higgins, J. M.; Jin, S. Chemical Synthesis and Magnetotransport of Magnetic Semiconducting $Fe_{1-x}Co_xSi$ Alloy Nanowires. *Nano Lett.* **2008**, *8*, 810–815.
19. Ouyang, L.; Thrall, E. S.; Deshmukh, M. M.; Park, H. Vapor-Phase Synthesis and Characterization of ε-FeSi Nanowires. *Adv. Mater.* **2006**, *18*, 1437–1440.
20. Hung, S. W.; Wang, T. T. J.; Chu, L. W.; Chen, L. J. Orientation-Dependent Room-Temperature Ferromagnetism of FeSi Nanowires and Applications in Nonvolatile Memory Devices. *J. Phys. Chem. C* **2011**, *115*, 15592–15597.
21. In, J.; Varadwaj, K. S. K.; Seo, K.; Lee, S.; Jo, Y.; Jung, M. H.; Kim, J.; Kim, B. Single-Crystalline Ferromagnetic $Fe_{1-x}Co_xSi$ Nanowires. *J. Phys. Chem. C* **2008**, *112*, 4728–4275.
22. Dietl, T.; Ohno, H.; Matsukura, F.; Cibert, J.; Ferrand, D. Zener Model Description of Ferromagnetism in Zinc-Blende Magnetic Semiconductors. *Science* **2000**, *287*, 1019–1022.
23. Pearton, S. J.; Abernathy, C. R.; Norton, D. P.; Hebard, A. F.; Park, Y. D.; Boatner, L. A.; Budai, J. D. Advances in Wide Bandgap Materials for Semiconductor Spintronics. *Mater. Sci. Eng. R* **2003**, *40*, 137–168.
24. Stowell, C. A.; Wiacek, R. J.; Saunders, A. E.; Korgel, B. A. Synthesis and Characterization of Dilute Magnetic Semiconductor Manganese-Doped Indium Arsenide Nanocrystals. *Nano Lett.* **2003**, *3*, 1441–1447.
25. Krstajiæ, P. M.; Peeters, F. M.; Ivanov, V. A.; Kikoin, K.; Fleurov, V. Double-Exchange Mechanisms for Mn-doped III-V Ferromagnetic Semiconductors. *Phys. Rev. B* **2004**, *70*, 195215.
26. Behan, A. J.; Mokhtari, A.; Blythe, H. J.; Score, D.; Xu, X.-H.; Neal, J. R.; Fox, A. M.; Gehring, G. A. Two Magnetic Regimes in Doped ZnO Corresponding to a Dilute Magnetic Semiconductor and a Dilute Magnetic Insulator. *Phys. Rev. Lett.* **2008**, *100*, 047206.
27. Teran, F. J.; Potemski, M.; Maude, D. K.; Plantier, D.; Hassan, A. K.; Sachrajda, A. Collective Character of Spin Excitations in a System of Mn^{2+} Spins Coupled to a Two-Dimensional Electron Gas. *Phys. Rev. Lett.* **2003**, *97*, 077201.
28. Dietl, T.; Ohno, H.; Matsukura, F. Hole-Mediated Ferromagnetism in Tetrahedrally Coordinated Semiconductors. *Phys. Rev. B* **2001**, *63*, 195205.
29. Manayala, N.; Sidis, Y.; Ditusa, J. F.; Aeppli, G.; Young, D. P.; Fisk, Z. Large Anomalous Hall Effect in a Silicon-Based Magnetic Semiconductor. *Nat. Mater.* **2004**, *3*, 255–262.
30. Jiang, W.; Zhou, X. Z.; Williams, G. Scaling the Anomalous Hall Effect: A Connection between Transport and Magnetism. *Phys. Rev. B* **2010**, *82*, 144424.
31. Schlesinger, Z.; Fisk, Z.; Zhang, H. T.; Maple, M. B. Is FeSi a Kondo Insulator? *J. Phys. B* **1997**, *13*, 460–462.
32. Beille, J.; Voiron, J.; Roth, M. Long Period Helimagnetism The Cubic B20 $Fe_xCo_{1-x}Si$ and $Co_xMn_{1-x}Si$ Alloys. *Solid State Commun.* **1983**, *47*, 399–402.
33. Uchida, M.; Onose, Y.; Matsui, Y.; Tokura, Y. Real-Space Observation of Helical Spin Order. *Science* **2006**, *311*, 359–361.
34. Mühlbauer, S.; Binz, B.; Jonietz, F.; Pfleiderer, C.; Rosch, A.; Neubauer, A.; Georgii, R.; Böni, P. Skyrmion Lattice in a Chiral Magnet. *Science* **2009**, *323*, 915–919.
35. Bauer, A.; Neubauer, A.; Franz, C.; Münzer, W.; Garst, M.; Pfleiderer, C. Quantum Phase Transitions in Single-crystal $Mn_{1-x}Fe_xSi$ and $Mn_{1-x}Co_xSi$: Crystal Growth, Magnetization, AC Susceptibility, and Specific Heat. *Phys. Rev. B* **2010**, *82*, 064404.

36. DeGrave, J. P.; Schmitt, A. L.; Selinsky, R. S.; Higgins, J. M.; Keavney, D. J.; Jin, S. Spin Polarization Measurement of Homogeneously Doped $Fe_{1-x}Co_xSi$ Nanowires by Andreev Reflection Spectroscopy. *Nano Lett.* **2011**, *11*, 4431–4437.
37. Paschen, S.; Felder, E.; Chernikov, M. A.; Degiorgi, L.; Schwer, H.; Ott, H. R.; Young, D. P.; Sarrao, J. L.; Fisk, Z. Low-Temperature Transport, Thermodynamic, and Optical Properties of FeSi. *Phys. Rev. B* **1997**, *56*, 12913–12930.
38. Manyala, N.; DiTusa, J. F.; Aeppli, G.; Ramirez, A. P. Doping a Semiconductor to Create an Unconventional Metal. *Nature* **2008**, *454*, 976–980.
39. Jeannine, R. S.; Jin, S. Epitaxially-Hyperbranched FeSi Nanowires Exhibiting Merohedral Twinning. *J. Mater. Chem.* **2010**, *20*, 1375–1382.
40. Higgins, J. M.; Carmichael, P.; Schmitt, A. L.; Lee, S.; Degrave, J. P.; Jin, S. Mechanistic Investigation of the Growth of $Fe_{1-x}Co_xSi$ ($0 \le x \le 1$) and $Fe5(Si_{1-y}Ge_y)_3$ ($0 \le y \le 0.33$) Ternary Alloy Nanowires. *ACS Nano* **2011**, *5*, 3268–3277.
41. Schmitt, A. L.; Bierman, M. J.; Schmeisser, D.; Himpsel, F. J.; Jin, S. Synthesis and Properties of Single-Crystal FeSi Nanowires. *Nano Lett.* **2006**, *6*, 1617–1621.
42. Tsai, C. I.; Wang, C. Y.; Tang, J.; Hung, M. H.; Wang, K. L.; Chen, L. J. Electrical Properties and Mangetic Response of Cobalt Germanosilicide Nanowires. *ACS Nano* **2011**, *5*, 9552–9558.
43. Hung, S. W.; Yeh, P. H.; Chu, L. W.; Chen, C. D.; Chou, L. J.; Wu, Y. J.; Chen, L. J. Direct Growth of β-$FeSi_2$ Nanowires with Infrared Emission, Ferromagnetism at Room Temperature, and High Magnetoresistance *via* a Spontaneous Chemical Reaction Method. *J. Mater. Chem.* **2011**, *21*, 5704–5709.
44. Chattopadhyay, M. K.; Roy, S. B.; Chaudhary, S. Magnetic Properties of $Fe_{1-x}Co_xSi$ Alloys. *Phys. Rev. B* **2002**, *65*, 132409.